Lineaments in Gravity Data of the Red Sea

Neil C. Mitchell

Abstract

The structure of the crust beneath the Red Sea is obscured by thick evaporites, impeding progress in understanding the processes associated with continental rifting and leaving the nature of the crust (whether oceanic or continental) still controversial. Here, version 18.1 of the marine gravity field derived from satellite altimetry measurements by Sandwell and Smith (1997) is examined because the gravity field has the potential to reveal structure associated with the topography of basement beneath the evaporites and with crustal density variations. Comparing the satellite-derived data with gravity data from expeditions of RRS *Shackleton* in 1979 and RV *Conrad* in 1984, discrepancies are found to have standard deviations of 6.1 and 4.9 mGal, respectively, somewhat higher than parts of the gravity data from the open oceans. Coherent features in maps of these discrepancies suggest that some systematic errors in version 18.1 of the gravity field still remain. Nevertheless, they appear not to affect the short-wavelength structure of the data because simple image processing reveals some striking structural features in plan-view. The satellite-derived gravity data are enhanced by showing them with artificial shading and as directional second derivatives. The maps reveal lineaments that cross the central Red Sea. Many of them die out towards the coastlines and have convex-north-west shapes. These features are interpreted as evidence for migrating volcanic segments of oceanic crust, here suggesting a 1.5 mm year^{-1} along-axis movement of the sub-axial asthenosphere away from the Afar plume. This migration velocity is modest compared with the plate-opening rate ($\sim$12 mm year^{-1} here) and compared with velocities deduced from V-shaped ridges near Iceland and the Azores.

Introduction

Resolving the structure beneath the Red Sea is important for addressing questions such as what type of crust lies beneath the sea and how oceanic fracture zones relate to structures on land. Of the former issue, Cochran (2005) and Cochran and Karner (2007) have argued convincingly that the northern Red Sea is floored by stretched continental crust, while other authors have shown that the crust in the southern Red Sea is probably mostly oceanic (Allan 1970; Cochran 1983; Roeser 1975; Vine 1966) except near the coasts (Egloff et al. 1991). In the intervening central Red Sea, high crustal velocities from seismic refraction experiments suggest that oceanic crust exists within about 65 km of the deeps (Davies and Tramontini 1970; Drake and Girdler 1964; Egloff et al. 1991; Tramontini and Davies 1969). The smooth character of a basement reflector in seismic reflection data also suggests oceanic crust (Izzeldin 1987). However, the lower amplitudes of magnetic anomalies away from the deeps may indicate instead that these are areas of continental crust (Bonatti 1985; Cochran 1983; Ligi et al. 2011, 2012, this volume).

In Mitchell and Park (2014), the depth of a crustal seismic refractor recorded in the central Red Sea east of Thetis Deep (Davies and Tramontini 1970; Tramontini and Davies 1969)

N.C. Mitchell (✉)
School of Earth, Atmospheric and Planetary Sciences, University of Manchester, Williamson Building, Oxford Road, Manchester M13 9PL, UK
e-mail: neil.mitchell@manchester.ac.uk

N.M.A. Rasul and I.C.F. Stewart (eds.), *The Red Sea*,
Springer Earth System Sciences, DOI 10.1007/978-3-662-45201-1_6,

was found to co-vary with free-air gravity anomalies derived from satellite altimetry data (Sandwell and Smith 2009). The rate of co-variation is compatible with the effect of topography of basement with a density contrast of crustal rocks with evaporites. This offers the possibility that marine gravity data can allow us to "see" through the evaporites to resolve some of the underlying structure.

Subsequent to the original data release of Sandwell and Smith (1997), their estimates of the free-air marine gravity field have improved with re-tracking of radar waveforms, better filtering methods and increasing coverage of the oceans by successive altimeter missions (Sandwell et al. 2013; Sandwell and Smith 2009). Although tracking error can be expected to be a problem in areas near coasts of narrow seas such as in the Red Sea, sea surface waves produce noise in altimeter data (Goff 2009), so the limited fetch and therefore smaller wave heights in the Red Sea than in broader oceans may partly compensate for the effect of tracking error. In the present study, version 18.1 of the data is studied, which is referred to as "SSv18".

The available terrestrial gravity field around the Red Sea has only modest resolution and is not useful for comparing with fine structure in the marine gravity field, so instead elevation data (Becker et al. 2009) derived from the Shuttle Radar Topography Mission (SRTM) were used in the present study to fill in land areas of the following maps. Strictly speaking, elevation data cannot be compared simply with gravity data because the topography of the Arabian-Nubian shield is the result of a long history of tectonics, erosion and other geological processes, whereas the gravity anomalies represent effects of topography of the crust under the Red Sea and variations in density and thickness of the crust. Nevertheless, the elevation data can provide some context for the offshore gravity data.

Datasets

Gravity data were collected on RRS *Shackleton* in 1987 with a LaCoste and Romberg marine gravity meter (Girdler and Southren 1987) and during RV *Robert Conrad* cruise 2507 in 1984 with a Bell BGM-3 (Cochran and Martinez 1988). Little information exists for the *Shackleton* data but, for the *Conrad* data, Cochran and Martinez (1988) found internal crossing errors of only 1 mGal in areas navigated by Loran-C and <3 mGal in the worst cases. (Given the "spikey" character of the *Conrad* data shown here, these values were presumably computed after data filtering.) These gravity data were obtained from the National Geophysical Data Center (www.ngdc.noaa.gov).

The SSv18 gravity field was sampled along the ship tracks, and the shipboard gravity measurements were then subtracted from those sampled values. The resulting differences are shown as profiles plotted towards N030°W in Figs. 1 and 2 for the *Shackleton* and *Conrad* cruises, respectively. Some spikes in Fig. 1 at the ends of lines appear to be mostly due to centripetal accelerations occurring with course changes. Given that other spikes occur in both datasets, the shipboard values were first filtered with a 4-km running median average filter before computing the statistics and other graphs outlined below. This 4-km filter width was necessary to ensure that a few samples populate the filter, whereas the theoretical spatial resolution limit of the marine gravity field is about equal to the depth to the density variations causing the anomalies (Turcotte and Schubert 1982), here 1–6 km depth below sea level to the evaporite/basement interface in the central Red Sea (Egloff et al. 1991; Izzeldin 1987, 1989; Tramontini and Davies 1969), so ~1–6 km

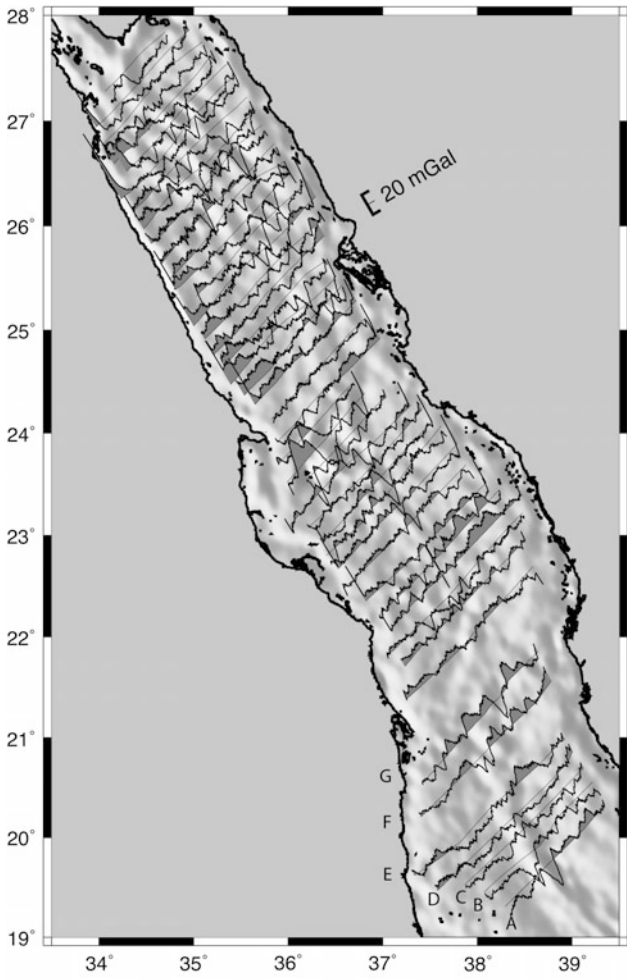

Fig. 1 Map of the Red Sea showing differences in free-air gravity anomaly between the Sandwell and Smith (2009) anomalies derived from satellite altimetry (SSv18) and the shipboard anomalies collected on RRS *Shackleton* (i.e., SSv18 minus the *Shackleton* data). The differences are plotted as profiles towards N030°W with the scale shown upper-right and with positive differences shaded. Background is a *shaded*-relief image of SSv18 illuminated from N060°E

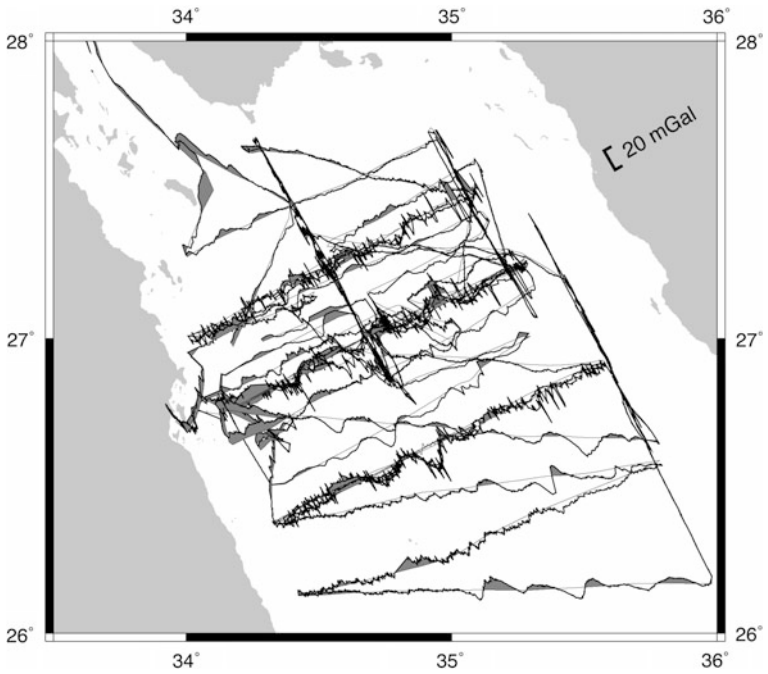

Fig. 2 Difference in free-air gravity anomaly between the SSv18 and the shipboard data collected on RV *Conrad* during cruise 2507, as Fig. 1

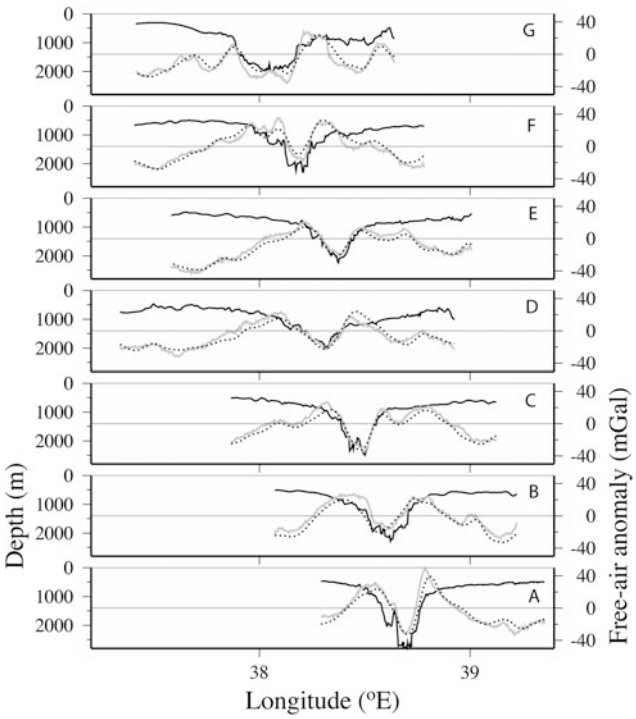

Fig. 3 Profiles of bathymetry (*bold lines*), free-air gravity shipboard measurements (*grey lines*) and free-air gravity sampled from SSv18 (*dotted lines*) for RRS *Shackleton* profiles (**A–G**) marked in Fig. 1

represent the range of the expected theoretical resolution. Figure 3 shows the shipboard and sampled gravity data along seven of the *Shackleton* profiles located in Fig. 1, revealing discrepancies over short wavelengths, including a tendency to flatten depressions or highs owing to the poorer resolution of the satellite-derived data.

In Fig. 4a, b, the variation of SSv18 with the filtered shipboard data is shown. The discrepancies between the two datasets are enlarged in Fig. 4c, d. Although the co-variation appears good, some large positive free-air anomaly (FAA) values have a negative bias and some large negative FAA values have a positive bias in the SSv18 data. This is an effect of the poorer resolution of the altimetry-derived data.

Figure 5 suggests that the differences are roughly normally distributed. The mean differences are −1.8 and −1.2 mGal in the *Shackleton* and *Conrad* data, respectively; note that these datasets have been reduced using different reference ellipsoids [International Association of Geodesy 1967 formula for the *Shackleton* data, Potsdam for the *Conrad* data and Earth Gravitational Model 2008 (Pavlis et al. 2012) for the SSv18 data (Sandwell and Smith 2009)]. The corresponding standard deviations are 6.1 and 4.9 mGal, the lower *Conrad* value possibly representing superior performance of the Bell BGM-3 gravity meter on the *Conrad* compared with the older LaCoste and Romberg meter that was installed on RRS *Shackleton*. These values are similar to the 5.6 mGal standard deviation found by Ligi et al. (2012) for a more limited area in the central Red Sea around Thetis Deep, but larger than differences between SSv18 and values from shipboard gravity in the open oceans, which have been shown locally to reach as small as 2.03 mGal (Sandwell and Smith 2009). Comparisons of the newer (version 21) gravity

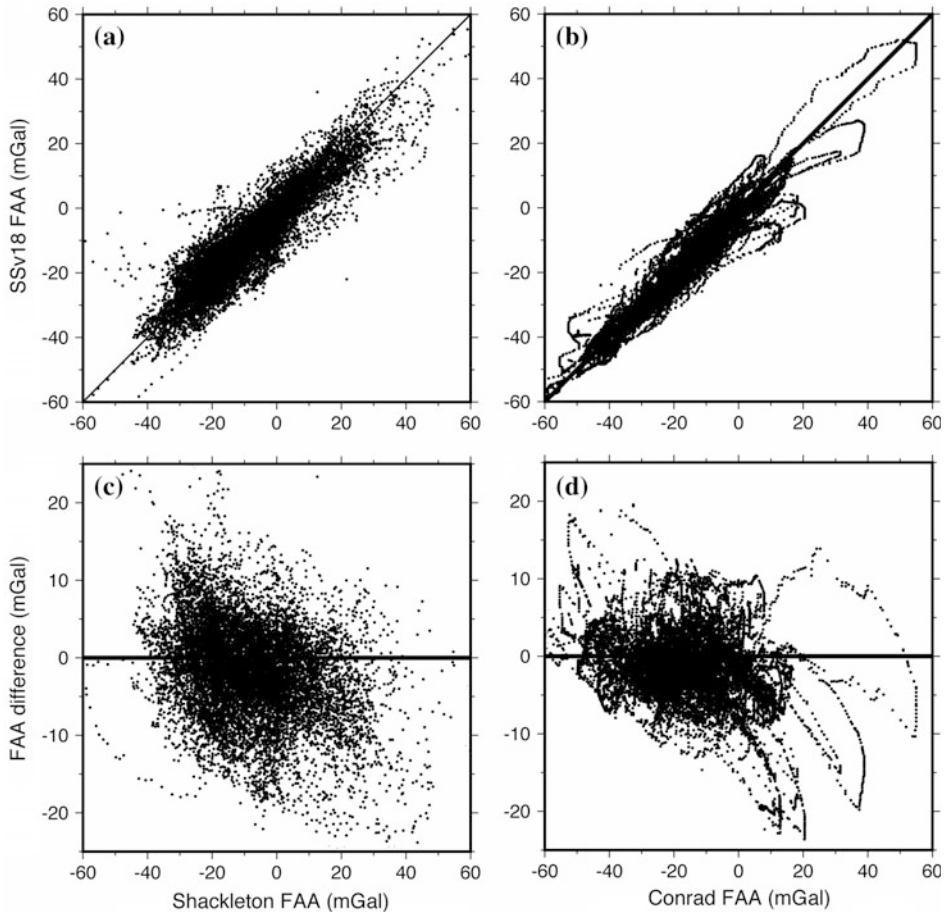

Fig. 4 Scatterplots of SSv18 free-air anomaly (FAA) versus shipboard values collected on **a** RRS *Shackleton* and **b** RV *Conrad*. Graphs **c** and **d** show differences between SSv18 and the shipboard values of (**a**) and (**b**), respectively (i.e., SSv18 minus shipboard value)

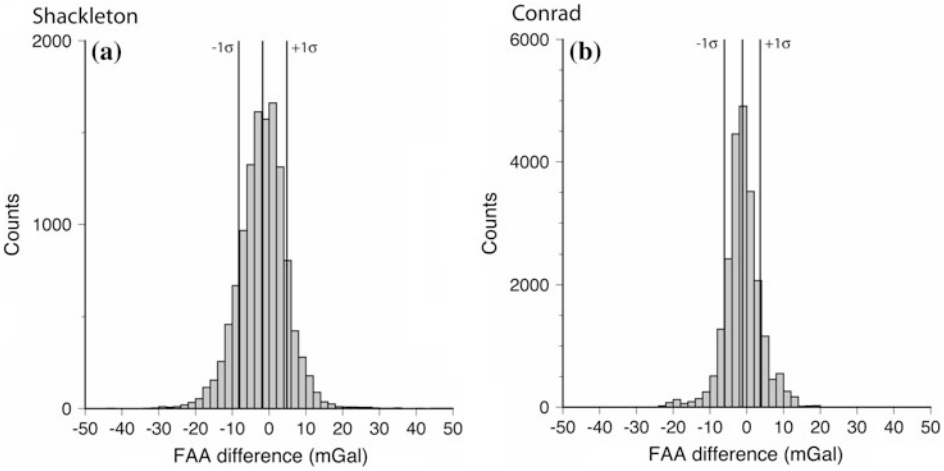

Fig. 5 Histograms of differences between the SSv18 and the shipboard free-air anomaly data from **a** RRS *Shackleton* and **b** RV *Conrad*. *Vertical lines* show the means and standard deviations of the differences

model with ship gravity measurements collected globally (National Geophysical Data Center data) by Sandwell et al. (2013) suggested a most likely median absolute difference of 2.75 mGal. For comparison with a dataset from another inland sea, a modest 2.35 mGal standard deviation was found between SSv18 and shipboard gravity data from Hudson Bay (Keating and Pinet 2013).

Somewhat more of a concern for structural studies, the difference maps in Figs. 1 and 2 show some non-random components (differences correlating between lines). Figure 6 is a colour-coded map of the differences. Whereas some narrow anomalies correlating between lines are probably caused by the satellite data resolution mentioned earlier (e.g. at 23.5°N mid-way between the coasts), large areas of blue

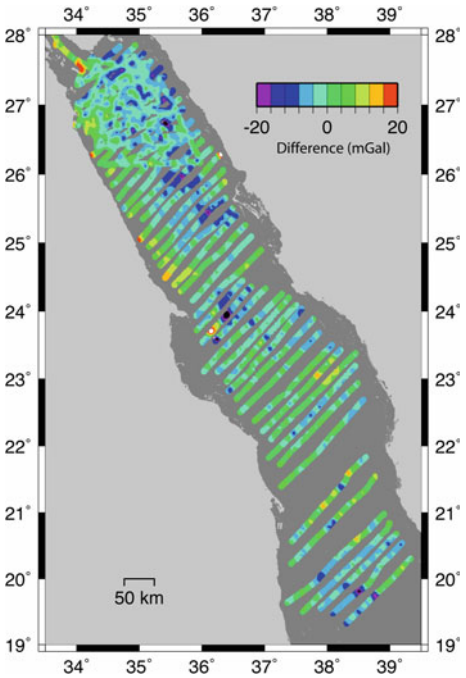

Fig. 6 Differences of the SSv18 gravity field and the *Shackleton* and *Conrad* shipboard gravity data (SSv18 minus shipboard). Shipboard data were first de-spiked with a 4-km along-track median filter

(−10 mGal difference) occur on the east side at 25°–26°N, centre at 24°N and south of the dataset south of 20°N. The 24°N central anomaly lies in an area of strong gravity field gradients (Styles and Gerdes 1983). Some coherent positive anomalies of +10 mGal occur close to the Egyptian coast. The magnitudes of these systematic biases are larger than those in the Hudson Bay study (Keating and Pinet 2013), where they typically reach only 4 mGal. Their origins are unclear. Sandwell (pers. comm. 2013) has suggested that these could be edge effects associated with converting altimetry deflections of the vertical offshore to gravity anomalies. Nevertheless, these anomalies are small compared with the >100 mGal full range of the SSv18 dataset and the appearance of structural features in the images presented below suggests that the gravity anomalies do not result in false structures appearing in plan-view.

Image Processing

To show elevations and the SSv18 data together, elevation values from the SRTM (Becker et al. 2009) were first rescaled so that the rescaled relief had a similar local variation to the gravity (a factor of 0.06 was found to achieve

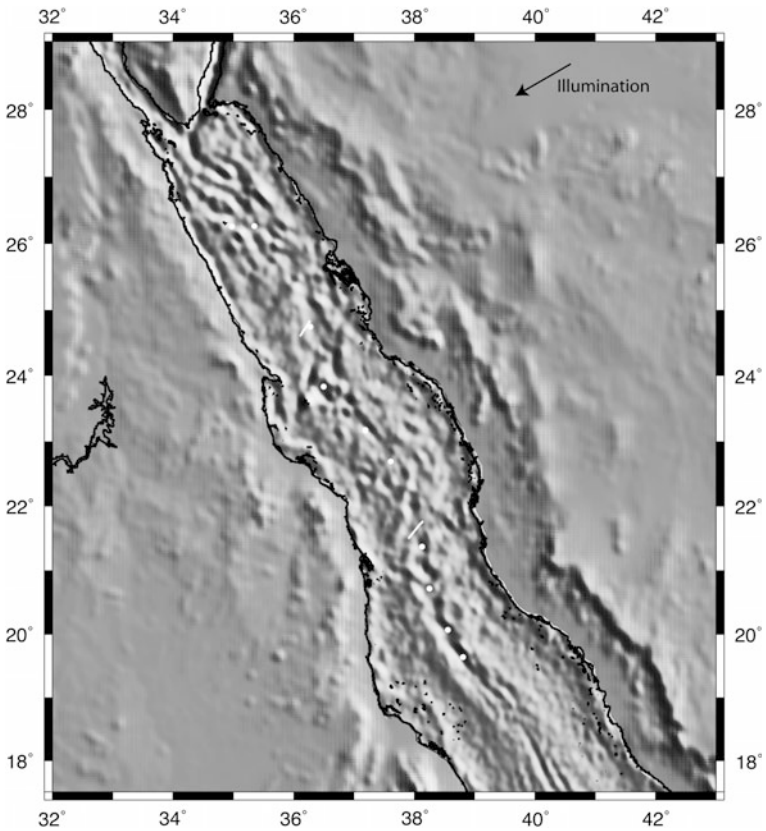

Fig. 7 The marine gravity field (SSv18) and land elevation data both shown in shaded relief with the artificial illumination from N060°E. Two *white bars* within the sea represent 3 m y of plate-tectonic movement predicted using the Chu and Gordon (1998) plate rotation pole. *Open circles* show a selection of the deeps of Pautot et al. (1984) to help readers locate features. From south to north, these are the Suakin, Port Sudan, Erba, Atlantis II, Thetis, Nereus, Vema, Kebrit, Jean Charcot and Oceanographer deeps

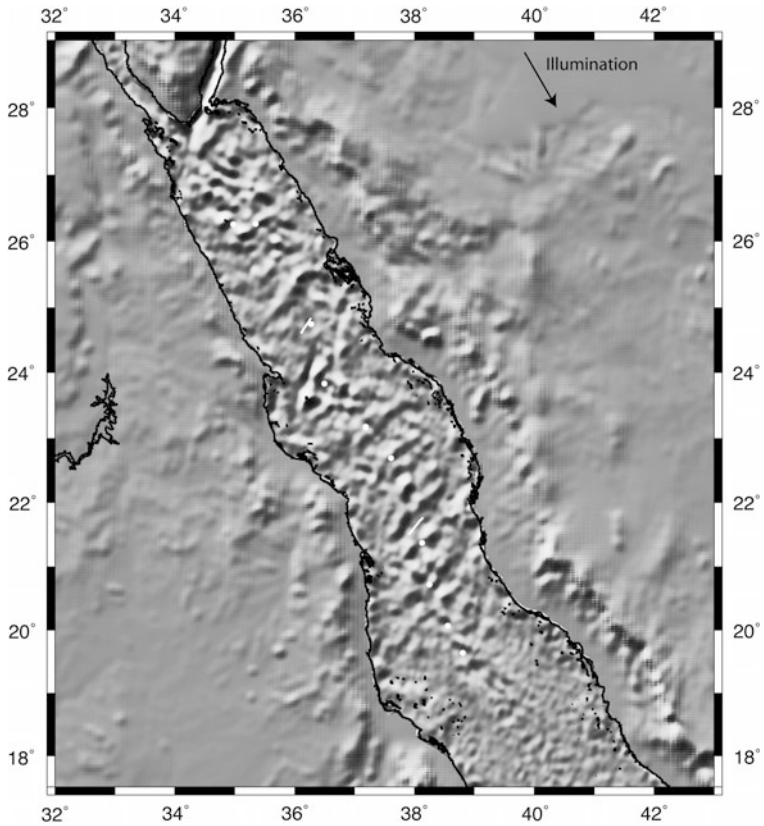

Fig. 8 As Fig. 7, with illumination from N030°W

visually the best result). Figures 7 and 8 show shaded-relief images of that combined dataset with the illumination directions shown in the upper-right in each figure. Before completing this operation, the elevation data were smoothed with a 0.25°-wide cosine-tapered two-dimensional filter to reduce the distraction of fine erosional geomorphology of escarpment gullies, etc. As the marine free-air gravity field is correlated with the relief of a basement refractor (Mitchell and Park 2014), basement structures beneath the evaporites should be correctly displayed with artificial illumination from the northerly compass direction (i.e., an apparent ridge in gravity should represent a ridge in the underlying basement, not a valley). The directional second derivatives shown in Figs. 9 and 10 were computed in a similar fashion, though with a grey-scale range that is narrower than the full range in order to enhance small curvature values representing more subtle data ridges or valleys.

A selection of the deeps given by Pautot et al. (1984) is shown by white and red dots on Figs. 7, 8, 9 and 10 so that readers can locate features on the maps (see caption of Fig. 7 for listing). To represent the trends expected of Nubia-Arabia plate motion, the Chu and Gordon (1998) plate rotation pole was used to rotate two points representing 3 m y of motion. The results are shown by white and red bars near 25°N and 22°N in Figs. 7, 8, 9 and 10.

Observations

Structures lying sub-parallel to the overall trends of the Red Sea and coasts are revealed in Figs. 7 and 9. Within the Red Sea north of 26°N, a series of NW–SE lineaments can be observed in Fig. 7. These correspond with the structures interpreted as continental rift blocks by Cochran (2005) [Compare also with the orientations of the extensional faults within Saudi Arabia in Figs. 3b and 6 of Bosworth (this volume)]. Elsewhere, Fig. 7 reveals longer lineaments mostly along the axis, although structures are visible near the Arabian coast at 22°N and on the African coast 22°–24°N and around Zabargad Island (near 24°N). The second derivative in Fig. 9 tends to enhance smaller inflections in both datasets to reveal further lineaments.

In Fig. 8, prominent transverse structures are visible within the Red Sea at 24°N (the Zabargad Fracture Zone) and 25°N. Further transverse structures are visible in the central Red Sea from 24°N to 20.5°N. At 20.5°N, a major lineament can be seen crossing the entire Red Sea and this feature is aligned with lineaments in elevation data on the surrounding land. A further lineament running N–S occurs in the marine gravity data on the Arabian side at 20°N and other lineaments on the corresponding African side, but

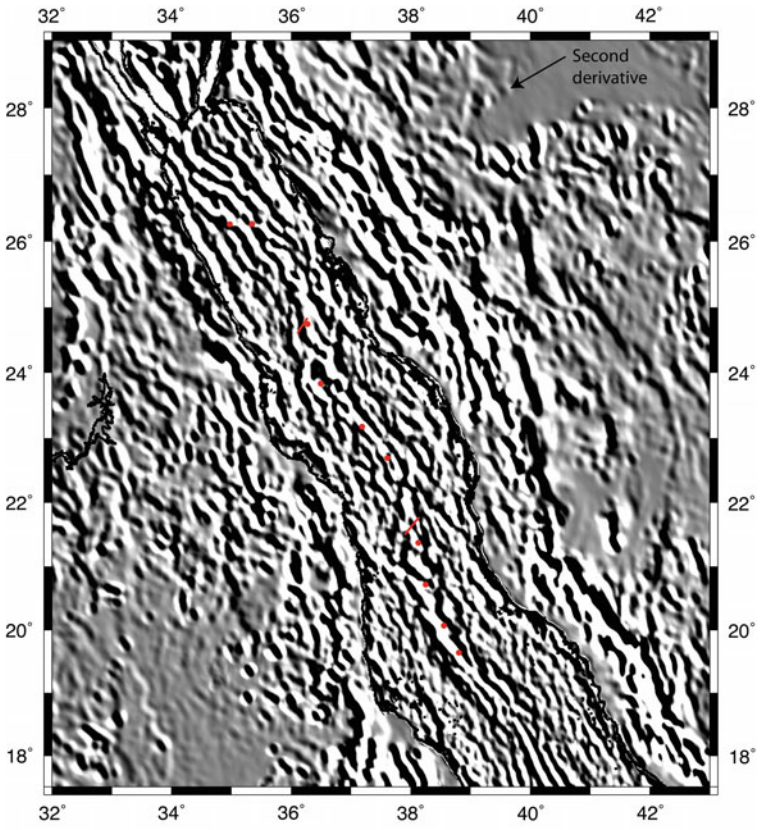

Fig. 9 Second derivative of SSv18 offshore and elevation data (Becker et al. 2009) onshore computed from N060°E (*black* represents downward-curved areas such as ridge crests and *white* represents upward-curved areas such as valleys or breaks in slope). *Red* annotation: 3 m y plate motion and deeps as Fig. 7

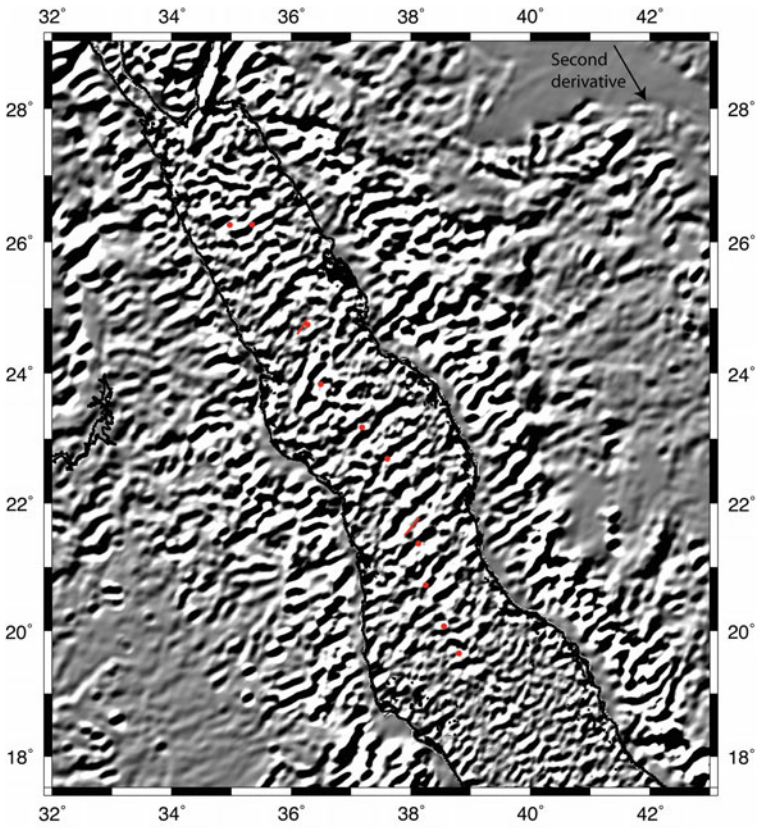

Fig. 10 Second derivative of SSv18 offshore and elevation data (Becker et al. 2009) onshore computed from N030°W. *Red* annotation: 3 m y plate motion and deeps as Fig. 7

otherwise lineaments are generally absent in the southerly part of the gravity dataset.

Discussion

Some transverse gravity lineaments appear to link with structures within the shields on land, in particular with two major ancient plate suture zones (Camp 1984; Stoeser and Camp 1985): the Halaib-Yanbu suture around 24°N and the Port-Sudan-Bi'r Umq suture around 20°N. These sutures coincide roughly with major protrusions of the Arabian coast and with indentations of the African coast.

The region south of 20°N has fewer transverse lineaments. A seismic refraction experiment carried out here by Egloff et al. (1991) revealed primarily oceanic crust and seismic reflection data show a subdued basement reflector (Izzeldin 1987). The Egloff et al. (1991) data show a 2-km-deep crustal depression in oceanic crust at the major transverse lineament at 20°N, which is therefore probably an oceanic fracture zone. The continuity of this feature makes it a good candidate for a continental structure that has directly led to the development of an oceanic transform fault.

Between there and 23°N, the transverse lineaments in the gravity data are generally less straight. Instead, they are slightly convex-NW, lying clockwise from the trend expected of plate motion on the Arabian side and anticlockwise of those trends on the Nubian side. In Fig. 8, the trends generally do not continue to the coast. This morphology is expected of non-transform discontinuities and volcanic segments on slow-spreading ridges, which tend to migrate in the direction expected of the mantle hot spot reference frame (Schouten et al. 1987) or away from hot spots (Briais and Rabinowicz 2002). In the case of the Red Sea, the migration is away from the Afar region, as expected if SAA is migrating north-westwards. Such a migration direction has been inferred from low seismic velocities extending north-west from Afar beneath the Red Sea in seismological studies of the upper mantle (Park et al. 2007).

The procedure of Schouten et al. (1987) can be used to estimate the rate of along-axis flow of SAA. In Fig. 11, the relative velocity of Nubia and Arabia is shown, computed from the rotation pole of Chu and Gordon (1998) for a point at 21.5°N on the axis (Fig. 7). Velocities along the spreading ridge are expected to lie along the dashed line in Fig. 11, which bisects the Nubia-Arabia velocity [assuming symmetrical spreading, which is suggested by the magnetic anomalies (Chu and Gordon 1998; Izzeldin 1987)] and with an orientation passing through the deeps. In contrast with Schouten et al. (1987), no distinction is made here between

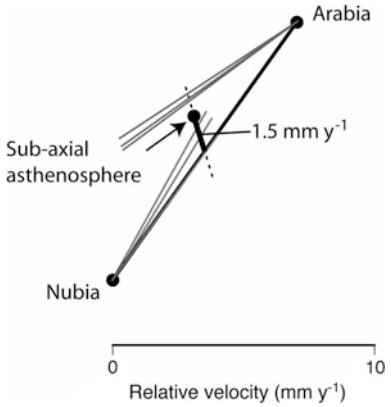

Fig. 11 Velocity-space diagram for the migrating segments of the central Red Sea. *Bold circles* marked Nubia and Arabia represent the relative separation of the two plates computed from the rotation pole of Chu and Gordon (1998) for a point at 21.5°N on the axis (*white bar* in Fig. 7). *Dashed line* represents velocities along the spreading ridge. *Grey lines* represent measured orientations of spreading segments. Remaining *bold solid circle* is the estimated SAA velocity

the mantle and SAA velocities. To estimate the direction of vectors between Nubia and SAA and between Arabia and SAA, the orientations of three segments were interpreted on either side of the axis from the near-axis trends in Fig. 8 (one segment immediately south of the white bar at 21.5°N and two segments north of there). Those orientations are shown by the grey lines in Fig. 11. The lines do not intersect along the dashed line, a result probably of the limited extents of data to make these measurements and data variability. Nevertheless, the velocity of the SAA can be estimated most likely to lie in the centre of the velocity space region encompassed by these lines along the dashed line, that is, at the solid circle marked "sub-axial asthenosphere" in Fig. 11. The velocity of SAA relative to the axis is thus around 1.5 mm year^{-1}, a slow rate compared with the plate velocities (around 12 mm year^{-1} full separation rate of Arabia and Nubia here (Chu and Gordon 1998).

To put this SAA movement in context relative to the Afar plume, Fig. 12 locates the central Red Sea area of migrating spreading segments on a three-dimensional view of the elevation data (Becker et al. 2009). The region of strongly elevated topography in Nubia and southern Arabia (higher than 1.5 km or red in Fig. 12) may reflect the northern-most region of magmatism and/or most important dynamic uplift and lithospheric heating by the Afar plume (Ebinger et al. 1989). The migrating segments lie to the north-west of this region. Comparison with evidence of the mantle plume from seismology is problematic because the present models of seismic velocity are derived from data with poor ray coverage under the Red Sea. Nevertheless, a study of shear-

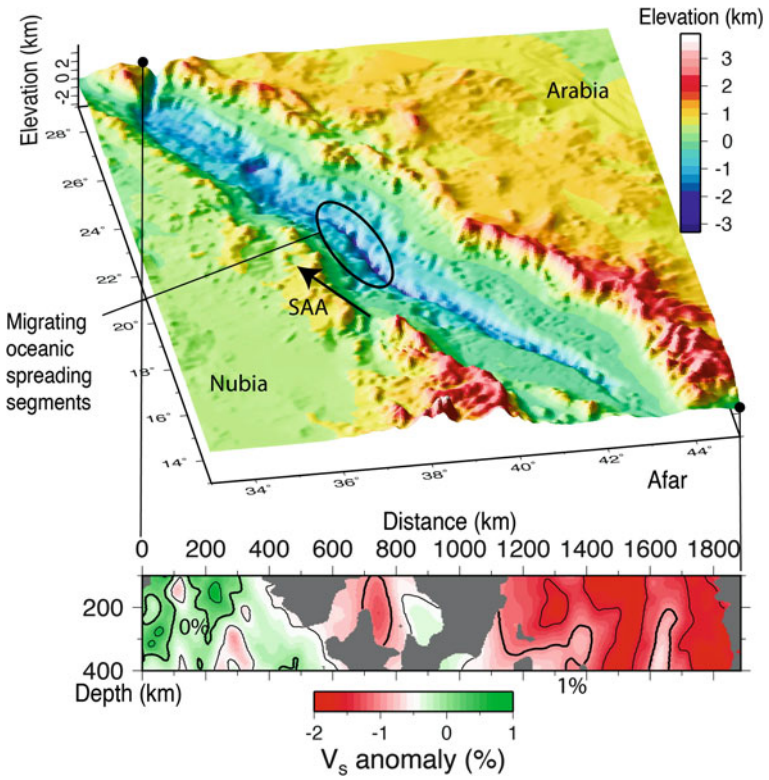

Fig. 12 Context of the proposed northward migrating oceanic spreading segments. Three-dimensional projection of the elevation/bathymetry model of Becker et al. (2009) is shown with the area of migrating segments marked (*ellipse*). These migrations imply a modest north-north-west velocity of the upper mantle (*arrow*). The central Red Sea corresponds with a region of the upper mantle with intermediate shear-wave velocities shown by the lower cross section, which is from a model of Park et al. (2007) based on teleseismic arrivals in Arabia. The velocity section is shown contoured every 0.5 % and represents structure between the two *solid circles* marked on the 3D view. *Grey* areas of section have poor teleseismic arrival constraints

wave velocity (V_s) by Park et al. (2007) was based on teleseismic arrivals recorded at stations distributed across Saudi Arabia and provides a view that is probably mimicked under the Red Sea. A vertical section of their model (Fig. 12) reveals a ~1.5 % increase in upper mantle V_s going north-west from southern Arabia beneath the coast. The area of migrating segments lies adjacent to intermediate V_s in the Park et al. (2007) model. Estimates of upper mantle temperature from sodium oxide contents of spreading centre lavas ("Na8.0") suggest a commensurate 60 °C decrease from 18°N to 26°N (Haase et al. 2000).

The area of modest 1.5 mm year^{-1} migration therefore appears to lie at the periphery of plume-influenced mantle. It also contrasts with regions of more rapid mantle velocity implied by V-shaped ridges around spreading centres (presumably located more proximal to their respective plumes). For example, such ridges around the Reykjanes Ridge suggest velocities away from the Icelandic plume of 87–282 mm year^{-1} (Poore et al. 2009) and those around the Mid-Atlantic Ridge south of the Azores suggest 60 mm year^{-1} (Cannat et al. 1999).

Conclusions

Simple image processing (shaded-relief and directional second derivatives or curvature) applied to version 18.1 of the marine gravity field of Sandwell and Smith (2009) reveals lineaments within the Red Sea, likely representing crustal structures beneath the evaporites. Lineaments crossing the central Red Sea are not straight and are more like migrating oceanic spreading segments observed elsewhere. Their orientations here imply a modest 1.5 mm year^{-1} migration of the SAA away from the Afar plume. Combined with other evidence of the region of influence of the plume (elevations, axial lava $Na_{8.0}$ and V_s from teleseismic arrivals in Arabia), the area of migrating lineaments lies at the periphery of the Afar plume.

Acknowledgments This project is largely based on data derived from satellite altimetry and generously provided online by David Sandwell and Walter Smith. Those researchers and the agencies providing the *Shackleton* and *Conrad* gravity data are thanked for making these data

freely available. The figures and many of the plate-tectonic and image processing calculations in this article were created or carried out with the "GMT" software system (Wessel and Smith 1991). Bill Bosworth kindly shared copies of geological maps of the Red Sea coasts and Yongcheol Park kindly gave a copy of his mantle V_s model. This work was initiated by discussions with Marco Ligi and Enrico Bonatti aboard RV *Urania* during a project on the Thetis Deep (Mitchell et al. 2010a, b). Jim Cochran and Walter Mooney are thanked for reviews of this paper. Najeeb M.A. Rasul and others of the Saudi Geological Survey are also thanked for an invitation to the enjoyable 2013 Red Sea workshop, which motivated this study.

References

Allan TP (1970) Magnetic and gravity fields over the Red Sea. Philos Trans R Soc A267:153–180

Becker JJ, Sandwell DT, Smith WHF, Braud J, Binder B, Depner J, Fabre D, Factor J, Ingalls S, Kim S-H, Ladner R, Marks K, Nelson S, Pharaoh A, Trimmer R, Von Rosenberg J, Wallace G, Weatherall P (2009) Global bathymetry and elevation data at 30 arc seconds resolution: SRTM30_PLUS. Mar Geodesy 32:355–371

Bonatti E (1985) Punctiform initiation of seafloor spreading in the Red Sea during transition from a continental to an oceanic rift. Nature 316:33–37

Briais A, Rabinowicz M (2002) Temporal variations in the segmentation of slow to intermediate spreading mid-ocean ridges. 1. Synoptic observations based on satellite altimetry data. J Geophys Res 107, Paper 2098. doi:10.1029/2001JB000533

Camp VE (1984) Island arcs and their role in the evolution of the western Arabian shield. Geol Soc Am Bull 95:913–921

Cannat M, Briais A, Deplus C, Escartín J, Georgen J, Lin J, Mercouriev S, Meyzen C, Muller M, Pouliquen G, Rabain A, da Silva P (1999) Mid-Atlantic Ridge-Azores hotspot interactions: along-axis migration of a hotspot-derived event of enhanced magmatism 10 to 4 Ma ago. Earth Planet Sci Lett 173:257–269

Chu D, Gordon RG (1998) Current plate motions across the Red Sea. Geophys J Int 135:313–328

Cochran JR (1983) A model for the development of the Red Sea. Am Assoc Petrol Geolo Bull 67:41–69

Cochran JR (2005) Northern Red Sea: nucleation of an oceanic spreading center within a continental rift. Geochem Geophysics Geosyst 6, Paper Q03006. doi:10.01029/02004GC000826

Cochran JR, Karner GD (2007) Constraints on the deformation and rupturing of continental lithosphere of the Red Sea: the transition from rifting to drifting. In: Karner GD, Manatschal G, Pinheiro LM (eds) Imaging, mapping and modelling continental lithosphere extension and breakup, Special Publication 282. Geological Society, London, pp 265–289

Cochran JR, Martinez F (1988) Evidence from the northern Red Sea on the transition from continental to oceanic rifting. Tectonophysics 153:25–53

Davies D, Tramontini C (1970) The deep structure of the Red Sea. Philos Trans R Soc A267:181–189

Drake CL, Girdler RW (1964) A geophysical study of the Red Sea. Geophys J Roy Astron Soc 8:473–495

Ebinger CJ, Bechtel TD, Forsyth DW, Bowin CO (1989) Effective elastic plate thickness beneath the East African and Afar plateaux and dynamic compensation of uplifts. J Geophys Res 94:2883–2901

Egloff F, Rihm R, Makris J, Izzeldin YA, Bobsien M, Meier K, Junge P, Noman T, Warsi W (1991) Contrasting structural styles of the eastern and western margins of the southern Red Sea: the 1988 SONNE experiment. Tectonophys 198:329–353

Girdler RW, Southren TC (1987) Structure and evolution of the northern Red Sea. Nature 330:716–721

Goff JA (2009) Statistical characterization of Geosat altimetry noise: dependence on environmental parameters. Geochem Geophys Geosyst 10, Paper Q08007. doi:10.1029/2009GC002569

Haase KM, Mühe R, Stoffers P (2000) Magmatism during extension of the lithosphere: geochemical constraints from lavas of the Shaban Deep, northern Red Sea. Chem Geol 166:225–239

Izzeldin AY (1987) Seismic, gravity and magnetic surveys in the central part of the Red Sea: their interpretation and implications for the structure and evolution of the Red Sea. Tectonophysics 143:269–306

Izzeldin AY (1989) Transverse structures in the central part of the Red Sea and implications on early stages of oceanic accretion. Geophys J 96:117–129

Keating P, Pinet N (2013) Comparison of surface and shipborne gravity data with satellite-altimeter gravity data in Hudson Bay. Lead Edge 32:450–458

Ligi M, Bonatti E, Tontini FC, Cipriani A, Cocchi L, Schettino A, Bortoluzzi G, Ferrante V, Khalil S, Mitchell NC, Rasul N (2011) Initial burst of oceanic crust accretion in the Red Sea due to edge-driven mantle convection. Geology 39:1019–1022

Ligi M, Bonatti E, Bortoluzzi G, Cipriani A, Cocchi L, Caratori Tontini F, Carminati E, Ottolini L, Schettino A (2012) Birth of an ocean in the Red Sea: initial pangs. Geochem Geophys Geosys 13, Paper Q08009. doi:10.1029/2012GC004155

Mitchell NC, Park Y (2014) Nature of crust in the central Red Sea and topographic control of evaporite flowage. Tectonophys. 628:123–139. doi:10.1016/j.tecto.2014.04.029

Mitchell NC, Ligi M, Farrante V, Bonatti E, Rutter E (2010a) Submarine salt flows in the central Red Sea. Geol Soc Am Bull 122:701–713.

Mitchell NC, Schmidt M, Ligi M (2010b) Comment on "Formation of thetis deep metal-rich sediments in the absence of brines, Red Sea" by Pierret. J Geochem Expl 108:112–113

Park Y, Nyblade AA, Rodgers AJ, Al-Amri A (2007) Upper mantle structure beneath the Arabian Peninsula and northern Red Sea from teleseismic body wave tomography: implications for the origin of Cenozoic uplift and volcanism in the Arabian Shield. Geochem Geophys Geosys 8, Paper Q06021. doi:10.1029/2006GC001566

Pautot G, Guennoc P, Coutelle A, Lyberis N (1984) Discovery of a large brine deep in the northern Red Sea. Nature 310:133–136

Pavlis NK, Holmes SA, Kenyon SC, Factor JK (2012) The development and evaluation of the Earth Gravitational Model 2008 (EGM2008). J Geophys Res 117, Paper B04406. doi:10.1029/2011JB008916

Poore H, White N, Jones S (2009) A Neogene chronology of Iceland plume activity from V-shaped ridges. Earth Planet Sci Lett 283:1–13

Roeser HA (1975) A detailed magnetic survey of the southern Red Sea. Geol Jahrb 13:131–153

Sandwell DT, Smith WHF (1997) Marine gravity anomaly from Geosat and ERS-1 satellite altimetry. J Geophys Res 102:10039–10054

Sandwell DT, Smith WHF (2009) Global marine gravity from retracked Geosat and ERS-1 altimetry: ridge segmentation versus spreading rate. J Geophys Res 114, Paper B01411. doi:10.1029/2008JB006008

Sandwell D, Garcia E, Soofi K, Wessel P, Chandler M, Smith WHF (2013) Toward 1-mGal accuracy in global marine gravity from CryoSat-2, Envisat, and Jason-1. The Leading Edge, pp 892–899

Schouten H, Dick HJB, Klitgord KD (1987) Migration of mid-ocean ridge volcanic segments. Nature 326:835–839

Stoeser DB, Camp VE (1985) Pan-African microplate accretion of the Arabian Shield. Geol Soc Am Bull 96:817–826

Styles P, Gerdes KD (1983) St. John's Island (Red Sea): a new geophysical model and its implications for the emplacement of ultramafic rocks in fracture zones and at continental margins. Earth Planet Sci Lett 65:353–368

Tramontini C, Davies D (1969) A seismic refraction survey in the Red Sea. Geophys J Roy Astron Soc 17:225–241

Turcotte DL, Schubert G (1982) Geodynamics: applications of continuum physics to geological problems. Wiley, New York 450 pp

Vine FJ (1966) Spreading of the ocean floor—new evidence. Science 154:1405–1415

Wessel P, Smith WHF (1991) Free software helps map and display data. Eos Trans Am Geophys Union 72:441